Record bandwidth and sub-picosecond pulses from a monolithically integrated mode-locked quantum well ring laser

Record bandwidth and sub-picosecond pulses from a monolithically integrated mode-locked quantum well ring laser

Valentina Moskalenko,* Sylwester Latkowski, Saeed Tahvili, Tjibbe de Vries, Meint Smit, and Erwin Bente

Department of Electrical Engineering, Technische Universiteit Eindhoven, De Dolech 2, 5612 AZ, Eindhoven, The Netherlands

v.moskalenko@tue.nl

Abstract: In this paper, we present the detailed characterization of a semiconductor ring passively mode-locked laser with a 20 GHz repetition rate that was realized as an indium phosphide based photonic integrated circuit (PIC). Various dynamical regimes as a function of operating conditions were explored in the spectral and time domain. A record bandwidth of the optical coherent comb from a quantum well based device of 11.5 nm at 3 dB and sub-picosecond pulse generation is demonstrated.

OCIS codes: (250.5590) Quantum-well, -wire and -dot devices; (140.4050) Mode-locked lasers; (130.0250) Optoelectronics; (140.5960) Semiconductor lasers; (250.5300) Photonic integrated circuits.

References and links

1. W. Drexler, "Ultrahigh-resolution optical coherence tomography," J. Biomed. Opt. **9**(1), 47–74 (2004).
2. K. Vlachos, N. Pleros, C. Bintjas, G. Theophilopoulos, and H. Avramopoulos, "Ultrafast time-domain technology and its application in all-optical signal processing," J. Lightwave Technol. **21**(9), 1857–1868 (2003).
3. G. Sansone, L. Poletto, and M. Nisoli, "High-energy attosecond light sources," Nat. Photonics **5**(11), 655–663 (2011).
4. A. D. Ellis and F. C. G. Gunning, "Spectral density enhancement using coherent WDM," IEEE Photon. Technol. Lett. **17**(2), 504–506 (2005).
5. J. Mandon, G. Guelachvili, and N. Picqué, "Fourier transform spectroscopy with a laser frequency comb," Nat. Photonics **3**(2), 99–102 (2009).
6. M. S. Tahvili, Y. Barbarin, X. J. M. Leijtens, T. de Vries, E. Smalbrugge, J. Bolk, H. P. M. M. Ambrosius, M. K. Smit, and E. A. J. M. Bente, "Directional control of optical power in integrated InP/InGaAsP extended cavity mode-locked ring lasers," Opt. Lett. **36**(13), 2462–2464 (2011).
7. J. S. Parker, A. Bhardwaj, P. R. A. Binetti, Y.-J. Hung, and L. A. Coldren, "Monolithically Integrated Gain-Flattened Ring Mode-Locked Laser for Comb-Line Generation," IEEE Photon. Technol. Lett. **24**(2), 131–133 (2012).
8. H. A. Haus, "Mode-locking of lasers," IEEE J. Sel. Top. Quantum Electron. **6**(6), 1173–1185 (2000).
9. Y. Barbarin, E. Bente, M. J. R. Heck, J. Pozo, J. M. Rorison, Y. S. Oei, R. Nötzel, and M. K. Smit, "18GHz Fabry-Pérot integrated extended cavity passively modelocked lasers," in Proc. ECIO, 2007, **vol. 7**, pp. 25–27.
10. K. A. Williams, M. G. Thompson, and I. H. White, "Long-wavelength monolithic mode-locked diode lasers," New J. Phys. **6**(1), 179 (2004).
11. J. Javaloyes and S. Balle, "Mode-Locking in Semiconductor Fabry-Perrot Lasers," IEEE J. Quantum Electron. **46**(7), 1023–1030 (2010).
12. Y. K. Chen, M. C. Wu, T. Tanbun-Ek, R. A. Logan, and M. A. Chin, "Subpicosecond monolithic colliding-pulse mode-locked multiple quantum well lasers," Appl. Phys. Lett. **58**(12), 1253–1255 (1991).
13. M. Smit, X. Leijtens, E. Bente, J. Van der Tol, H. Ambrosius, D. Robbins, M. Wale, N. Grote, and M. Schell, "Generic foundry model for InP-based photonics," IET Optoelectron. **5**(5), 187–194 (2011).
14. Joint European Platform for Photonic Integration of InP-based Components and Circuits." [Online]. Available: http://www.jeppix.eu/.
15. V. Moskalenko, J. Javaloyes, S. Balle, M. K. Smit, and E. A. J. M. Bente, "Theoretical Study of Colliding Pulse Passively Mode-Locked Semiconductor Ring Lasers With an Intracavity Mach-Zehnder Modulator," IEEE J. Quantum Electron. **50**(6), 415–422 (2014).

#217017 - $15.00 USD Received 16 Jul 2014; revised 16 Sep 2014; accepted 20 Oct 2014; published 11 Nov 2014

16. J. Parker, P. Binetti, A. Bhardwaj, R. Guzzon, E. Norberg, Y.-J. Hung, and L. Coldren, "Comparison of Comb-line Generation from InGaAsP/InP Integrated Ring Mode-locked Lasers," in CLEO:2011 - Laser Applications to Photonic Applications, 2011, p. CTuV6.
17. R. Rosales, S. G. Murdoch, R. T. Watts, K. Merghem, A. Martinez, F. Lelarge, A. Accard, L. P. Barry, and A. Ramdane, "High performance mode locking characteristics of single section quantum dash lasers," Opt. Express **20**(8), 8649–8657 (2012).
18. G.-H. Duan, A. Shen, A. Akrout, F. V. Dijk, F. Lelarge, F. Pommereau, O. LeGouezigou, J.-G. Provost, H. Gariah, F. Blache, F. Mallecot, K. Merghem, A. Martinez, and A. Ramdane, "High performance InP-based quantum dash semiconductor mode-locked lasers for optical communications," Bell Labs Tech. J. **14**(3), 63–84 (2009).
19. Y. Takushima, H. Sotobayashi, M. E. Grein, E. P. Ippen, and H. A. Haus, "Linewidth of mode combs of passively and actively mode-locked semiconductor laser diodes," **5595**, Proc. SPIE, 213–227 (2004).
20. T. Habruseva, S. O'Donoghue, N. Rebrova, F. Kéfélian, S. P. Hegarty, and G. Huyet, "Optical linewidth of a passively mode-locked semiconductor laser," Opt. Lett. **34**(21), 3307–3309 (2009).
21. D. A. Reid, S. G. Murdoch, and L. P. Barry, "Stepped-heterodyne optical complex spectrum analyzer," Opt. Express **18**(19), 19724–19731 (2010).
22. A. Otani, T. Otsubo, and H. Watanabe, "Chromatic dispersion measurement of EDFA using optical sampling oscilloscope," Optical Fiber Communication Conference and Exhibit, OFC 98," Technical Digest **1998**, 255–256 (1998).

1. Introduction

Passive mode-locking is one of the techniques which allows for the generation of broad coherent optical combs and short optical pulses. Both properties of such passively mode-locked lasers (PMLL) found application in various scientific and industrial areas. Short optical pulses are widely used in high resolution imaging [1], optical signal processing [2] and time-resolved measurements [3]. Due to the high spectral density and coherence of the laser modes the PMLL can be considered as a promising source for wavelength-division multiplexing systems [4] or high speed spectroscopy [5]. Semiconductor mode-locked lasers bring additional advantages in terms of wide optical gain, stability, footprint, and power consumption. Furthermore in the framework of optical integration technology, such a laser can be realized as a part of an optical system on a single monolithic chip which can be fabricated at relatively low costs [6], [7].

The simplest semiconductor PMLL can be formed by combining a saturable absorber (SA) and semiconductor optical amplifier (SOA) in a Fabry-Perot waveguide resonator. The SOA provides the optical gain which can be saturated. The SA provides self-amplitude modulation of the light inside the cavity through its saturation of absorption at lower intensities than the saturation of the SOA. The combination of these two saturation processes leads to optical pulse formation [8]. However the use of such a two-section Fabry-Perot quantum well (QW) and bulk laser is often limited either by the relatively long pulse durations of 2-5 ps, a limited operating parameter region of stable operation or a small coherent optical bandwidth [9], [10].

In order to bring this area forward active-passive integration technology can be used. This technology allows for more advanced laser designs where passive components are included. In this case the length of the SOA and the SA are to a large extent decoupled from the resonator length which determines the repetition rate. This helps to reduce the issue of amplitude modulations [9] and self-phase modulation as observed in all-active two-section devices. In [7] it was shown that optical bandwidth and pulse duration can be significantly improved by introducing intra-cavity passive wavelength dependent filter. Another advantage of this technology is that the relative position of the SA and SOA and output coupler in the cavity can be optimized, e.g. to control the relative power in the two directions in a ring cavity [6].

The quality of PMLL performance strongly depends on the geometrical properties of the laser components, in particular the lengths of the SA and SOA. In [11] it was shown theoretically that optimal mode-locking in terms of optical comb and pulse duration can be achieved only in a limited range of ratios between the SOA and SA length. Previously [6] an integrated extended cavity symmetrical ring semiconductor PMLL fabricated within our

#217017 - $15.00 USD Received 16 Jul 2014; revised 16 Sep 2014; accepted 20 Oct 2014; published 11 Nov 2014

active-passive integration platform was demonstrated by our group. However, its pulse duration was in the order of 3-4 ps and optical comb bandwidth didn't exceed 3 nm. In this paper we present the characterization results of a ring semiconductor PMLL with an improved design. We demonstrate a bandwidth of more than 11.5 nm and sub-picosecond optical output pulses. We also present a detailed study of the PMLL performance in temporal and spectral domains at various operating conditions.

2. Mode-locked ring laser geometry

The configuration of the 20 GHz ring PMLL studied in this paper is shown in Fig. 1. In this configuration two pulses propagate in the cavity in opposite directions and collide in the SA, saturating it simultaneously. Due to the deep absorber saturation the colliding pulse configuration allows for stable sub-picosecond optical pulse generation [12]. In linear laser configuration this technique is very sensitive to the position of SA, whereas in the ring cavity SA can be located freely. Another reason for using the ring configuration is that the repetition rate which is determined by the length of the cavity can be controlled more accurately than that of a Fabry-Perot type laser with cleaved facets.

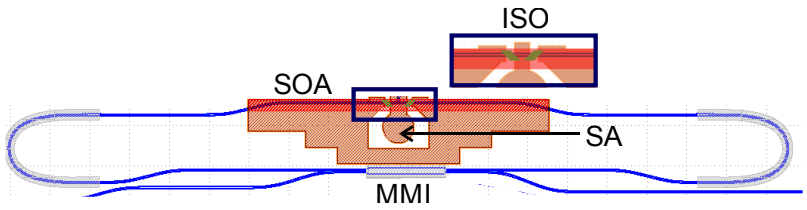

Fig. 1. Mask layout of a symmetrical ring PMLL. SOA – semiconductor optical amplifier, SA - saturable absorber, ISO – two electrical isolation sections (shown in green), MMI - multimode interference coupler, AR – anti-reflection coating. The total length of the cavity was 4 mm.

The device was fabricated using an InP generic integration technology platform. The platform uses shallowly and deeply etched ridge waveguides that are 2.0 and 1.5 μm wide respectively and butt-joint technology with one regrowth step and one overgrowth step to achieve the active-passive integration [13]. The layer stack has a 500 nm thick InGaAsP Q = 1.25 waveguiding layer. The wafer included predefined areas containing an active core with four InGaAs quantum wells (QW) and 20 nm barriers in between. Therefore the SOA and the SA sections had to be located inside such an area, whereas passive components must be placed outside of it. The chip was fabricated within a multiproject wafer (MPW) run at COBRA through the Jeppix foundry coordinator [14]. The 4 mm long laser cavity (Fig. 1) includes two 345 μm long SOA sections and a 30 μm saturable absorber section which are separated by two 15 μm isolation sections, a multi-mode interference coupler (MMI) and passive waveguides. The MMI and the bends at both sides of the ring are deeply etched waveguides, all other sections are shallow ridge waveguides. In order to provide carriers for both SOA sections using a single bias current source the contacts of the two SOA sections share a single metal electrode. An MMI coupler provides 3 dB out-coupling in both directions, which allows for equal power distribution among the two-counter propagating pulses. The relative position of the SOAs and SA was designed such that both pulses will experience the same amplification and meet in the SA. In order to minimize possible back reflections coming from the edges of the chip the output waveguides were positioned at 7° with respect to the cleaved and AR-coated facets. The intra cavity reflections were reduced by using angled active-passive interfaces, adiabatic bends, an optimized MMI structure and deep to shallow waveguide transitions. Compared to the device presented in [6], the laser presented in this paper includes a SA section that is 10 μm longer. The use of a longer SA allows for reduction of risk of the chip getting damaged due to the high Joule heating in the reversely

#217017 - $15.00 USD Received 16 Jul 2014; revised 16 Sep 2014; accepted 20 Oct 2014; published 11 Nov 2014

biased SA generated by the photocurrent. Therefore the laser can be operated over an extended range of operating conditions.

3. Optical coherent comb

The device was mounted on a temperature-controlled copper chuck which was used to keep the temperature at 18° C during the measurements. Light from both outputs was collected using lensed fibers with antireflection coating. Optical isolators were used to prevent back reflections into the laser cavity. The performance of the PMLL was investigated in three ways: by observation of optical spectra which show the comb of the longitudinal modes simultaneously existing in the cavity, measurement of RF beat signals of these modes on a fast photodiode and observation of the time domain second harmonic autocorrelation intensity profile using an autocorrelator in a background free configuration. The optical spectra were measured using a high resolution (20 MHz) optical spectrum analyzer (OSA). The RF tones were produced on a 55 GHz photodiode (PD) and were recorded by a 50 GHz bandwidth electrical spectrum analyzer (ESA). In order to investigate the laser performance in time domain autocorrelation traces were recorded. Due to the low output power the signal was first amplified by a low noise erbium doped fiber amplifier (EDFA) and then sent through the polarization controller (PC) to autocorrelator. The influence of EDFA on output signal is discussed later.

The laser was operated by reverse biasing the SA and forward biasing the SOA sections. In [11], [15] it was shown theoretically that the performance of a mode-locked laser is very sensitive to many factors such as recovery time of the SA and SOA, gain bandwidth and the relative shift between absorption and amplification spectra, which varies for different operating conditions. In order to investigate and to find the conditions for optimal passively mode-locked operation, the laser was characterized over a wide range of SA voltages and SOA injected currents.

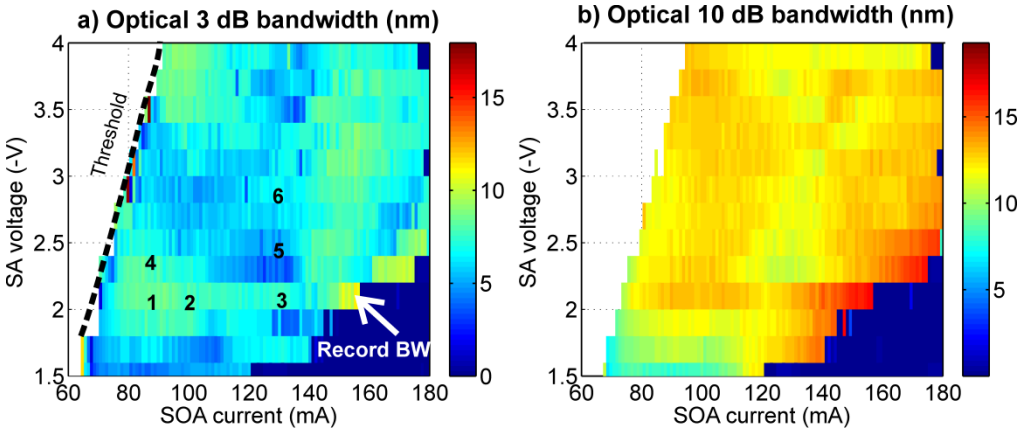

Fig. 2. A map of the spectral bandwidth measured at 3 dB (a) and 10dB (b) level as a function of biasing conditions applied to the SOA and SA sections. Numbers indicate operating points at which the output pulses were characterized in detail.

The configuration of output waveguides allowed for the signal to be collected from both facets. In the mode-locking range of operating conditions the signals from both directions show similar performance in terms of coupled optical power, distribution of optical modes and RF spectrum. All results presented below were obtained for the signal collected from the same facet. Figure 2 shows maps of the width of the optical spectrum at 3 dB (a) and 10 dB (b) level as a function of bias conditions. Due to the changes in the shape of optical spectra with bias conditions Fig. 2(b) shows a more homogeneous distribution of the bandwidth over the bias conditions compared to the one presented in Fig. 2(a).

#217017 - $15.00 USD Received 16 Jul 2014; revised 16 Sep 2014; accepted 20 Oct 2014; published 11 Nov 2014

RF spectra have been recorded for the same operating points as were used in optical spectra measurements. Figures 3(a) and 3(b) shows examples of full span RF spectra for various operating regimes. The RF spectrum in Fig. 3(a) shows a clear peak at the fundamental frequency 20 GHz, which corresponds to the roundtrip time and second harmonic at 40 GHz. Figures 3(c) and 3(d) present in detail the RF spectra around the fundamental frequency when mode-locking is occurring. Figure 3(c) shows a RF peak with 1.6 MHz 10 dB linewidth. Figure 3(d) shows an example when amplitude modulations are present. The 10 dB linewidth in this case is 7 MHz. The electrical spectrum recorded at I_{BIAS} = 166 mA and U_{SA} = –3.8 V shows low-frequency components, which are indication of Q-switching instabilities.

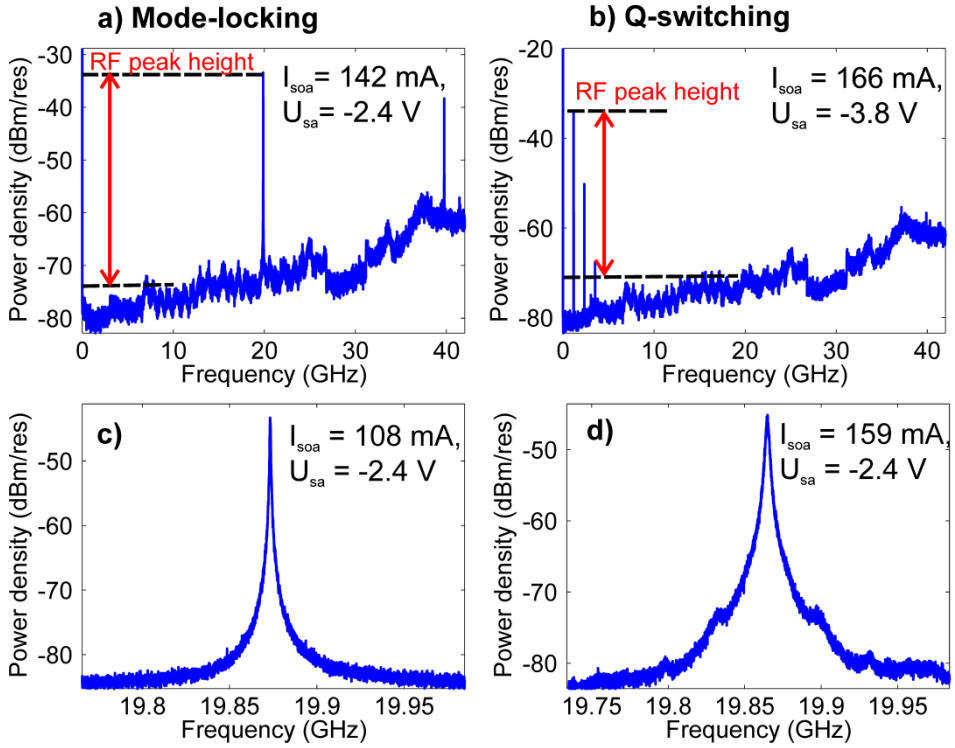

Fig. 3. Examples of measured RF spectra for various operating regimes. (a) RF spectrum measured at I_{BIAS} = 142 mA and U_{SA} = –2.4 V which is in the mode-locking regime. b) RF spectrum measured at I_{BIAS} = 166 mA and U_{SA} = –3.8 V. At these bias conditions the laser exhibits Q-switching instabilities. Detailed RF spectra recorded at (c) I_{BIAS} = 108 mA and U_{SA} = 2.4 V and (d) I_{BIAS} = 159 mA and U_{SA} = –2.4 V show mode-locking and mode-locking with amplitude modulations (AM) respectively.

Figure 4(a) shows a map of the height of the RF peak as a function of I_{BIAS} and U_{SA}. Height of RF peak value was taken as a ratio between the peak at fundamental frequency 20 GHz and low frequency components as shown in Fig. 3 (a) and 3(b). The areas where the peak at 20 GHz was observed clearly are indicated as the red and dark red colors. Variation in RF peak height can be explained by differences in output power and by the presence of enhanced low frequency noise (amplitude modulation). The areas with amplitude modulations (AM) are indicated by a white dashed line. Notice, that mode-locking with AM was also observed near the edge of stable mode-locking at high injected currents. An RF linewidth in the region of stable mode-locking varies from 1 to 7 MHz at 10 dB level. In the regions where AMs were observed the linewidth increases up to 40 MHz.

#217017 - $15.00 USD Received 16 Jul 2014; revised 16 Sep 2014; accepted 20 Oct 2014; published 11 Nov 2014

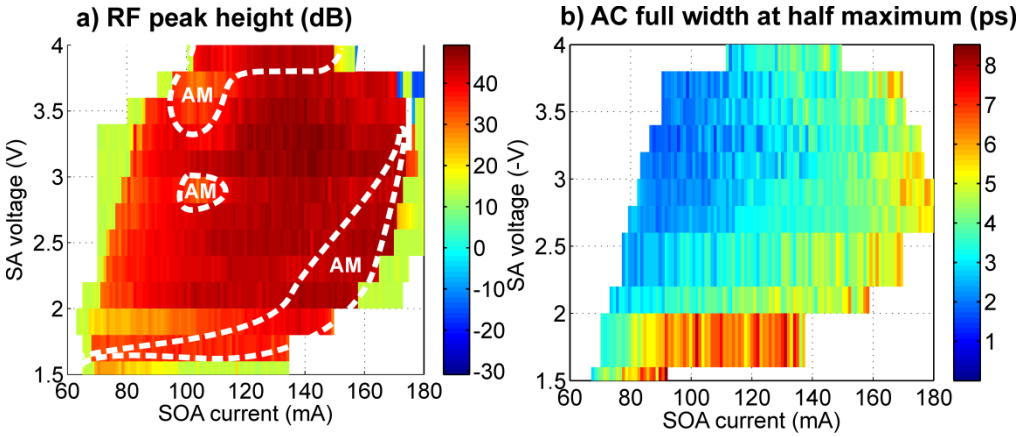

Fig. 4. (a) A map of the RF peak height measured at the same set of operating conditions as in Fig. 2. Areas outlined by a dashed white line correspond to the operating conditions range where mode-locking with amplitude modulation (AM) was observed. (b) Map of the autocorrelation trace full width at half maximum at the same set of operating conditions as in (a).

The right-top corner of the picture indicates the region of the negative values (blue). This means that low-frequency spectral components (between 25 MHz and 3 GHz) are present and exceed the RF peak value at the fundamental frequency. The laser is then in a passively Q-switched dynamical state. A laser can exhibit Q-switching instabilities when the saturation processes in the gain and the SA are not balanced within in one roundtrip. In our case Q-switching was observed at relatively high values of I_{BIAS} and U_{SA}. Then the SA becomes fully saturated in the onset of a pulse while the gain section is not and still has enough carriers to provide further amplification. The high voltage on the SA makes that the gain in the SOA can recover to high small-signal gain values before a new pulse is formed.

As a characteristic of the time domain PMLL performance the width of the autocorrelation (AC) trace was used. All time traces were obtained for the same autocorrelator settings of 50 ps scan range with 260 data points, which correspond to a 200 fs time resolution in the autocorrelation signal. Figure 4(b) shows the AC full width at half maximum (FWHM) as a function of injected current and applied voltage. Pulse formation was observed in the regions indicated in the contour plot where the color indicates the AC FWHM. The shortest pulses (FWHM < 4 ps) were obtained at the relatively low injected currents (the darkest blue zone) close to the lasing threshold. A further increase of the current leads to increase of optical power and therefore increasing self-phase modulation effects due to increasing gain saturation in the SOA. Starting from certain current levels in the SOA the AC trace width values (FWHM) presented in Fig. 4(b) do not show the pulse broadening which can be attributed to the appearance of satellite pulses.

The widest optical comb was observed at I_{BIAS} = 154.8 mA and U_{SA} = –2 V and is presented in Fig. 5(a). This operating point is indicated in Fig. 2(a) with a white arrow. It features an FWHM bandwidth of 11.5 nm (1.41 THz) and a bandwidth of 17 nm (2.16 THz) when measured at –10 dB. These are record values when compared to the results obtained from devices with a similar geometry and based on QW material as presented up to date [7], [16]. The values are comparable to those reported from quantum dash based lasers [17], [18]. The high resolution of the optical spectrum analyzer (down to 20 MHz) allowed for measurements of a linewidth directly from the optical spectrum. The linewidths of modes are represented as red circles and values are shown on the left axis. In [19] and [20] it was shown experimentally that in passively mode-locked semiconductor lasers timing jitter dominates over the carrier envelope phase noise and the optical linewidth depends on the square of the mode number with the minimum at the central wavelength. At low current densities (up to

#217017 - $15.00 USD Received 16 Jul 2014; revised 16 Sep 2014; accepted 20 Oct 2014; published 11 Nov 2014

approximately 1.5 times the threshold current) we observe, that the spectral linewidth dependency partly has a parabolic shape (Fig. 6(f)). The central modes show linewidth values that are limited at approximately 800 MHz, which is much wider than the linewidth reported in [7]. The broadening of central modes shown in Fig. 5(a) means that the phases of these modes are not perfectly locked. Increase of the injection current leads to a change of dynamic regime which results in the appearance of AM of the pulse train and linewidth broadening at the central part of the optical spectrum (Fig. 5(a)). This would indicate a further reduction of the quality of phase locking of the modes at the center. However, future studies of this effect are required.

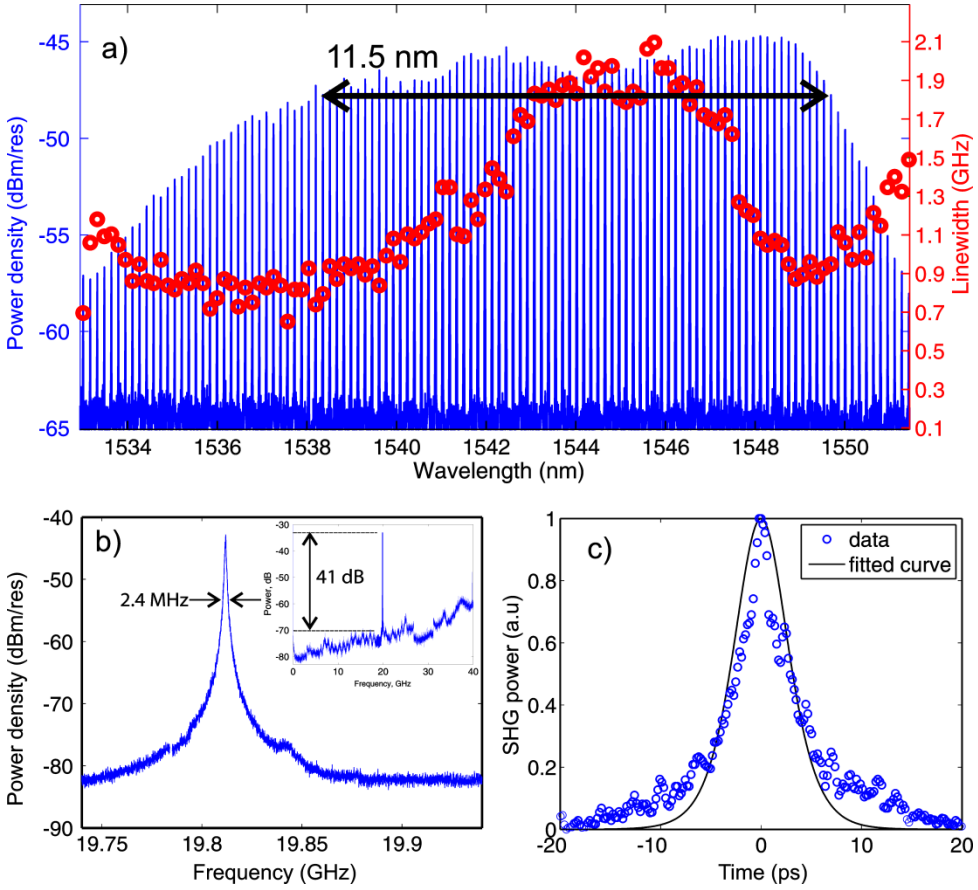

Fig. 5. (a) The optical frequency comb recorded at I_{BIAS} = 154.8 mA and U_{SA} = –2 V with a 3 dB bandwidth of 11.5 nm (1.41 THz). Red circles represent the linewidth values for each mode. (b) RF spectrum at I_{BIAS} = 154.8 mA and U_{SA} = –2 V: The RF peak shows the fundamental frequency of the 4 mm long cavity. Inset: Broadband RF spectrum showing low frequency noise components. (c) Autocorrelation trace (blue circles) fitted by $sech^2$ profile (black curve) at I_{BIAS} = 154.8 mA and U_{SA} = –2 V.

The electrical spectrum from the photodiode (Fig. 5(b)) at these bias conditions shows a clear peak at 19.81 GHz. The observed peak had a 40 dB height and a 2.4 MHz width measured at –10 dB (~800 kHz at FWHM). Figure 5(c) presents the AC trace (blue circles) fitted by $sech^2$ (black curve) at the same injected current and applied voltage. The extracted pulse duration was 3.8 ps. Notice, that the recorded autocorrelation profile is not in a good agreement with the fitting curve and the pulse is expected to show a considerable amount of chirp.

#217017 - $15.00 USD Received 16 Jul 2014; revised 16 Sep 2014; accepted 20 Oct 2014; published 11 Nov 2014

In order to characterize the intensity and phase profile of the output pulses in detail a stepped-heterodyne technique was used. This method was described in [21] and it allows for the measurement of the amplitude and phase of the pulse in the time domain without the need of additional amplification and thus without deformation of the pulse caused by propagation in the erbium doped fiber amplifier.

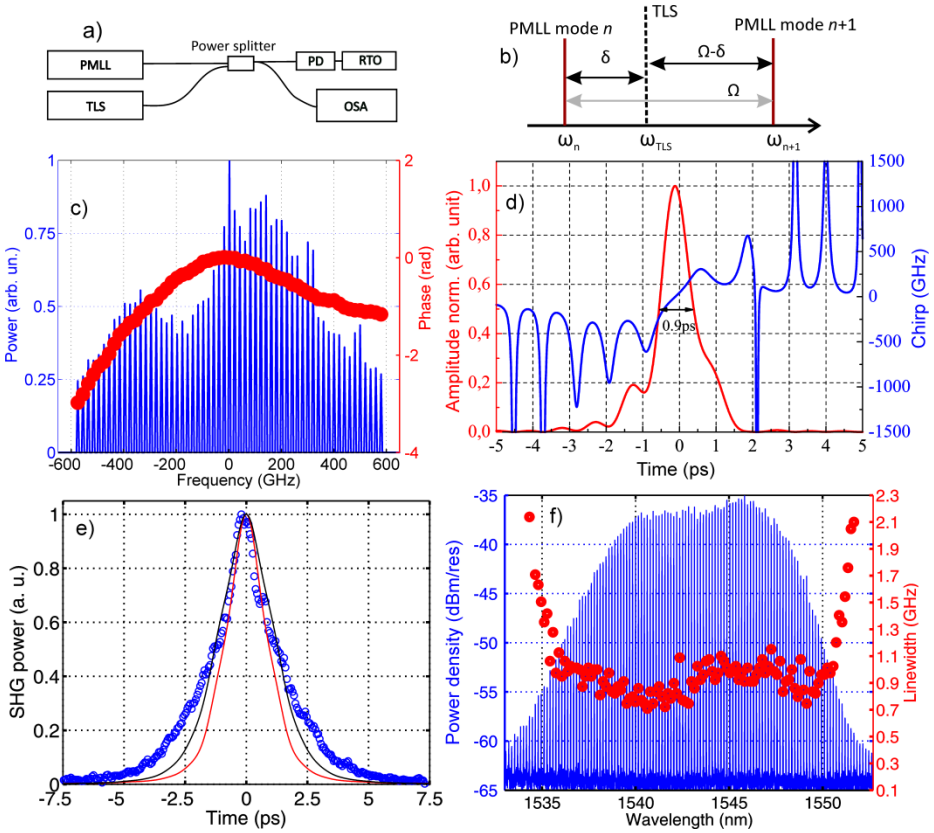

Fig. 6. a) Sketch of the setup for the stepped-heterodyne technique. TLS – tunable laser source, PD – photodetector, RTO – real-time oscilloscope, OSA – optical spectrum analyzer. b) PMLL neighboring modes ω_n and ω_{n+1}, TLS mode ω_{TLS} and the offsets between them δ, Ω and Ω-δ. c) Optical spectrum (blue) in linear scale and phase (red) measured using stepped-heterodyne method at I_{BIAS} = 90 mA and U_{SA} = –2 V. d) Optical pulse chirp (blue) and amplitude (red) profile measured using the stepped-heterodyne method. The RMLL is biased at I_{BIAS} = 90 mA and U_{SA} = –2 V. e) Measured AC trace (blue circles) at I_{BIAS} = 90 mA and U_{SA} = –2 V. AC traces calculated from the amplitude and phase profile shown in (d) with (black) and without (red) taking into consideration a dispersion and gain of EDFA used for amplification of the signal during measurements. f) The optical frequency comb recorded at I_{BIAS} = 90 mA and U_{SA} = –2 V. Red circles represent the linewidth values for each mode.

In this technique the PMLL optical pulse is combined with the light from a tunable laser source (TLS). The schematic setup is shown in Fig. 6(a). The beating frequencies between TLS and two neighboring laser modes as well as beats of all PMLL modes together are generated on the fast photodiode (PD). A real time oscilloscope (RTO) with 50 GHz bandwidth was used to record time traces which include the electromagnetic field amplitude oscillations on beating frequencies δ, Ω-δ and Ω as shown in Fig. 6(b). In order to retrieve the information of phase and amplitude, the signals at δ, Ω-δ and Ω are digitally filtered, and signals at δ and Ω-δ are multiplied together. The phase difference between the component of this multiplied signal at Ω and the original filtered signal at Ω contains the phase difference information between the two neighboring modes. By tuning the TLS across the whole laser

#217017 - $15.00 USD Received 16 Jul 2014; revised 16 Sep 2014; accepted 20 Oct 2014; published 11 Nov 2014

output spectrum and by repeating the procedure described above for each mode a complete phase spectrum can be obtained. The amplitude of each spectral mode can be extracted from the amplitude of the filtered signal at δ. Figure 6(c) shows the optical comb (blue) in linear scale and phase (red) that were obtained using the stepped-heterodyne technique at I_{BIAS} = 90 mA and U_{SA} = −2 V. These operating conditions are indicated in Fig. 2(a) as point 1. The spectral phase shows non-linear distribution over the optical frequency and varies in 3 rad range. Figure 6(d) shows the pulse amplitude and chirp profiles calculated from the data showed in Fig. 6(c). Pulse duration of 900 fs and a chirp of 350 GHz (across the pulse duration) was observed. It is to be noted that in the obtained graph the central part of the pulse has a chirp with a linear time dependency which can be compensated. The calculated group delay required for this is 1.15 ps over a 10 nm wavelength range. In the case of constant phase distribution over the entire spectrum the pulse width would be limited only by the spectral shape (the optical spectrum obtained at the same operating conditions is shown in Fig. 6(f)) and will be narrowed down to 800 fs.

Since we used a CW tunable laser with 500 kHz line width the signal at δ or Ω-δ can be also used for calculation of the linewidth of each optical mode. The left axis of the plot in Fig. 6 (f) shows the optical linewidths which were measured using the high resolution optical spectrum analyzer. These data are in a good agreement with the linewidths determined using the stepped-heterodyne method described above. Notice from Fig. 6(f) that the linewidth (red circles) of the spectral modes is on average lower than the ones presented in Fig. 5(a) obtained at higher injected currents.

The measurements of pulse amplitude and phase were performed for several operating points, which are indicated in Fig. 2(a) as numbers from 1 to 6. Remaining operating points (2 - 6 in Fig. 2 (a)) showed longer and more severely chirped optical pulses in comparison with operating point 1 discussed above. Obtained pulse durations were 3.59 ps, 3.81 ps, 1.06 ps, 2 ps and 1.62 ps for the points 2, 3, 4, 5, 6 respectively. However, a chirp compensation can in principle reduce pulse durations down to 0.82 ps, 0.7 ps, 0.62 ps, 0.58 ps and 0.72 ps for these points.

Despite the clear advantages of the stepped-heterodyne method it is not feasible for characterization of the whole range of the operating conditions. In order to characterize one operating point a set of time traces with the TLS tuned between each mode pair in the output spectrum has to be recorded. Each individual time trace consists of around 2.4 million data points and the whole data set has to be processed and analyzed off-line, which makes the procedure extremely time consuming.

In Fig. 4(b) we presented experimentally obtained AC FWHM for a wide range of operating conditions obtained. In order to examine these results, we compare the AC functions that were calculated using the amplitude shown in Fig. 6(d) with the measured autocorrelation trace for the same bias conditions. The measured AC time trace was measured with a 15 ps scan and a 60 fs time resolution. This trace is presented in Fig. 6 (e) with blue circles. The red curve in Fig. 6(e) corresponds to the calculated background free AC signal using the measured pulse amplitude profile. The black curve is a calculated AC signal that also includes the additional phase offsets and the spectrally non-uniform amplification caused by the propagation through the EDFA. This information was added to each longitudinal mode pulse amplitude and phase as determined in the stepped heterodyne measurement. The length of the EDFA fiber was 42 m with 10.8 ps/(nm·km) as the value of the dispersion parameter [22]. The non-uniform amplification by the EDFA was measured. Figure 6(e) shows that the propagation of the optical signal through the erbium-doped fiber leads to the pulse broadening which results in broadening of the autocorrelation trace from 1.9 ps to 2.6 ps. The experimental autocorrelation trace shows 2.3 ps full width at half maximum. Notice that this number differs from the one shown in Fig. 4(b) at this operating condition. The use of a shorter time scan range on the autocorrelator allows for a higher resolution and therefore more precise results.

#217017 - $15.00 USD Received 16 Jul 2014; revised 16 Sep 2014; accepted 20 Oct 2014; published 11 Nov 2014

The FWHM of the recorded AC signal and the AC signal calculated from the stepped heterodyne measurement are in good agreement with each other. However, the AC signal obtained from the autocorrelator is more broadened at intensities below the 50% level. Such differences in shapes of the AC signal can be explained by a large range of small changes in the wings of the optical pulse.

3. Conclusions

A ring geometry 20 GHz passively mode-locked laser realized as a PIC fabricated within a generic InP foundry has been demonstrated. The use of the longer SA section allowed to increase the range of injected currents and applied voltages in comparison with [6]. In this range of operating conditions a stable mode-locking region with more than 40 dB height of the RF peak at the fundamental frequency over the low frequency noise was observed. The laser output showed an optical bandwidth of up to 11.5 nm and optical pulses down to 900 fs long. The operating region for stable mode-locking is surrounded by the areas of mode-locking with increased low frequency noise. Autocorrelation measurements showed broadening of the pulse with an increase of injected current, which can be explained by the increase of self-phase modulation effects. Increase of injected current also leads to an optical mode broadening. This dynamic regime of the laser needs further investigation. Q-switching was observed outside these regions of operating conditions.

In this paper we demonstrated an optical coherent comb with a 3 dB bandwidth of 11.5 nm which is the widest reported optical comb for QW based PMLLs. Using a stepped-heterodyne technique the phase and amplitude in the spectral and temporal domain were obtained at several operating points. The PMLL has shown a pulse that was 900 fs wide with a linear chirp over 350 GHz across the central part of the pulse. The pulse duration was confirmed by the analysis of autocorrelation trace at the same operating point.

#217017 - $15.00 USD Received 16 Jul 2014; revised 16 Sep 2014; accepted 20 Oct 2014; published 11 Nov 2014